SIGNIFICANCE OF THERMAL BOUNDARY LAYER ANALYSIS OF MHD CHEMICALLY RADIATIVE DISSIPATIVE CASSON NANOFLUID FLOW OVER A STRETCHING SHEET WITH HEAT SOURCE

By

SEETHARAM KARANAMU * JAYARAMIREDDY KONDA ** SHAIK KALESHA VALI ***

** Department of Mathematics, Aditya Institute of Technology and Management, Tekkali, Srikakulam, Andhra Pradesh. India.*
*** Science City, Government of Andhra Pradesh, Tadepalli, Guntur District, Andhra Pradesh, India.*
**** Department of Basic Science & Humanities and Social Sciences, JNTUK University College of Engineering Vizianagaram, Dwarapudi, Vizianagaram, Andhra Pradesh, India.*

Date Received: 20/06/2023 *Date Revised: 04/07/2023* *Date Accepted: 05/08/2023*

ABSTRACT

A mathematical model that incorporates thermal emission, glutinous indulgence, heat source/sink, substance response, with suction was used to learn the MHD pour of Casson nanofluid in excess of a nonlinearly porous stretched page. There are a series of nonlinear ordinary differential equations that govern the biased differential equations through proper resemblance transformations, as well as then solved by the Homotopy Analysis Approach (HAM). Numerical data and plots are employed to examine the physical limitations on liquid speed, heat, and attentiveness. To examine the flow characteristics at the wall, the skin friction coefficients, local Nusselt digit, and Sherwood numbers are in addition evaluated. With much acclaim, a link between penetrable findings for specific cases is discovered.

Keywords: Nanofluid of Casson, Thermal Emission, Heat Generation/Absorption, Suction, Viscous Dissipation, HAM.

INTRODUCTION

When a magnetic field is applied to a magnetic-fluid, a fundamental phenomenon called magnetic interaction occurs. It has been widely recognized in a variety of fields of research, including magnetic field alignment, particle separation, and nanocrystal manipulation, among others. Abel et al. (2008) investigated the flow and heat transfer behavior of viscoelastic fluid over a stretching surface under the impact of viscous and ohmic dissipation. Kumaran et al. (2009) found the perfect solution for an electrically conducting fluid flowing through a boundary layer past a quadratically stretched and linearly permeable sheet. The thermal radiation effect on MHD flow across an exponentially stretched sheet was discussed by Mabood et al. (2017a). Later on many problems have been discussed by few authors (Ibrahim et al., 2017; Kumar et al., 2018; Reddy & Sreedevi, 2021; Mabood et al., 2015; Reddy & Shankar, 2016; Kumar et al., 2017).

Because non-Newtonian fluids have broad uses in modern industrial and technical products, many researchers are focusing on their exploration these days. Food, ketchup, shampoos, slurries, granular suspension, paper pulp, paints, polymer solutions, some oils, and clay coatings are just a few examples of non-Newtonian materials. A single mathematical connection cannot identify all of the characteristics of non-Newtonian liquids. Casson fluid model Casson (1959) is a prominent model for many fluids such as blood, chocolate, honey, etc. Casson fluid acts as solid when the shear stress is less than the yield stress and it starts to deform when shear stress becomes greater than the yield stress. Dash et al. (1996) investigated the behavior of Casson fluid under yield stress through a homogeneous porous medium bounded by circular tube. Mukhopadhyay (2013) studied flow and heat transfer characteristics of Casson fluid over a nonlinear stretching surface. Mustafa and Khan (2015) discussed the magnetic field effect on Casson nanofluid over a nonlinearly stretching sheet.

Nanofluids are one of the most exciting areas of current research because of their enormous promise for improved heat transmission. Choi and Eastman (1995) was the first to coin the word "nanofluid" to designate a new category of fluid. Masuda et al. (1993) described the phenomena of thermal conductivity augmentation as the key distinctive feature of nanofluids. The strengthening of the heat transmission rate with regular carrier liquids is highlighted in distinct scholarly articles (Mabood et al., 2017b; Kumar et al., 2019; Mabood et al., 2017b; Nadeem et al., 2013).

In fluid mechanics, viscous dissipation is a term used to describe the extinction of oscillatory velocity gradients caused by viscous strains. This partially irreversible phenomenon is referred to as the transfer of kinetic energy into internal energy of the fluid. Energy dissipation and non-Newtonian fluid flow are also fascinating to engineers and scientists. According to Pop (2010) understanding energy dissipation and transport in nanoscale structures is critical for designing energy-efficient circuits and energy-conversion devices. Energy dissipation and non-Newtonian fluid flow are also fascinating to engineers and scientists. Ajayi et al. (2017) looked at the effects of viscous dissipation in a non-Newtonian Casson fluid flow across the upper horizontal thermally stratified melting surface of a paraboloid of revolution. Khan et al. (2020) looked into how partial slip influenced Williamson stagnation nanofluid flow over a stretching/shrinking surface. In the fluid flow phenomenon, the outcomes of thermal radiation and heat transfer are crucial. Some recent study about non-Newtonian and nanofluid in different geometries with diverse properties are in (Rao et al., 2020; Kumar et al., 2018; Mopuri et al., 2022a; Mopuri et al., 2022b; Mohyuddin & Rizwan, 2015; Asghar et al., 2005; Mohyuddin & Götz, 2005).

In this article, we analyzed the MHD boundary layer flow of Casson nanofluid which is obtained from the nonlinear porous stretching of a sheet using HAM (Kumar et al., 2021; Ibrahim et al., 2018; Ibrahim et al., 2019; Ibrahim et al., 2020; Liao, 2012; Hayat et al., 2012). In this study we considered suction, magnetic field, thermal radiation, viscous dissipation, heat generation/absorption and chemical reaction.

There are non-Newtonian fluids and nanofluids that combine the Casson and nanofluid models in terms of physical properties. As a result, these fluids can be described as a Casson-nanofluid model, as in our study, which is based on previous nanofluid model researches [36]. The above studies did not take into account the impact of both viscous dissipation and chemical reaction, as well as the effects of mixed convection and nanoparticles, on the mass and heat transfer strategy for non-Newtonian nanofluids induced by stretching sheets embedded in porous media. As far as the authors are aware, no other published research on this area has been attempted. The novelty of this study is based on the efficiency of chemical reactions caused by nanoparticle movements in the presence of heat generation, as well as viscous dissipation for a non-Newtonian Casson-nanofluid model subjected to magnetic field, thermal radiation, and chemical reaction in a porous media.

1. Mathematical Formulation

Consider a steady, two dimensional and incompressible mixed convection MHD flow of a Casson nanofluid located at $y=0$. The flow is confined to $y>0$ and the sheet is stretched along the x-axis with velocity $U_w = ax^n$, where $n\geq 0$ is a nonlinear stretching parameter and $a>0$ is a constant. The fluid is electrically conducted due to an application of magnetic field $B(x) = B_0 x^{(n-1/2)}$ normal to the sheet. The magnetic Reynolds number is assumed small and so the induced magnetic field can be considered to be negligible. It is assumed that T_w and C_w are the wall temperature and nanoparticle concentration and as $y\to\infty$, the ambient values of temperature and nanoparticle fraction are T_∞ and C_∞ such that $T_w>T_\infty$ and $C_w>C_\infty$. The rheological equation of state for an isotropic and incompressible flow of a Casson fluid is,

$$\tau_{ij} = \begin{cases} 2\left(\mu_B + \dfrac{p_y}{\sqrt{2\pi}}\right)e_{ij}, & \pi > \pi_c \\ 2\left(\mu_B + \dfrac{p_y}{\sqrt{2\pi_c}}\right)e_{ij}, & \pi_c > \pi \end{cases}$$

where μ_B is the dynamic viscosity of the non-Newtonian fluid, p_y is the yield stress of the fluid, π is the product of the

component of deformation rate with itself, $\pi = e_{ij}e_{ij}$, e_{ij} is the $(i,j)^{th}$ component of the deformation rate and π_c is the critical value of this product based on the non-Newtonian model. The velocity field is taken as V=[u(x,y), v(x,y), 0]. Under the boundary layer approximations, the governing equations for conservation of mass, momentum, thermal energy and nanoparticle concentration of this problem can be expressed. Yousif et al. (2017) have defined Neglecting buoyancy forces, edge effects, pressure gradient presence and the conservation equations i.e. mass, momentum, energy and nano-particle species conservation equations, and the following may be presented as,

$$\frac{\partial u}{\partial x}+\frac{\partial v}{\partial y}=0, \tag{1}$$

$$u\frac{\partial u}{\partial x}+v\frac{\partial u}{\partial y}=\nu\left(1+\frac{1}{\beta}\right)\frac{\partial^2 u}{\partial y^2}-\frac{\sigma B^2(x)}{\rho_f}u-\frac{\nu}{K}u \tag{2}$$

$$u\frac{\partial T}{\partial x}+v\frac{\partial T}{\partial y}=\alpha\frac{\partial^2 T}{\partial y^2}+\frac{(\rho c)_p}{(\rho c)_f}\left[D_B\frac{\partial C}{\partial y}\frac{\partial T}{\partial y}+\frac{D_T}{T_\infty}\left(\frac{\partial T}{\partial y}\right)^2\right]+\frac{\nu}{C_p}\left(1+\frac{1}{\beta}\right)\left(\frac{\partial u}{\partial y}\right)^2-\frac{1}{(\rho c)_f}\frac{\partial q_r}{\partial y}+\frac{1}{(\rho c)_f}\frac{Q_0}{(T-T_\infty)} \tag{3}$$

$$u\frac{\partial C}{\partial x}+v\frac{\partial C}{\partial y}=D_B\frac{\partial^2 C}{\partial y^2}+\frac{D_T}{T_\infty}\frac{\partial^2 T}{\partial y^2}-k_0(C-C_\infty) \tag{4}$$

Subject to the boundary conditions

$$\begin{aligned} &u=U_w=a\,x^n,\quad v=v_w,\quad T=T_w,\quad C=C_w \ \ at\ \ y=0,\\ &u\to 0, v\to 0,\ \ T\to T_\infty, C\to C_\infty \qquad\qquad as\ \ y\to\infty. \end{aligned} \tag{5}$$

Following Rosseland approximation, the radiative heat flux is,

$$q_r=-\frac{4\sigma^*}{3k^*}\frac{\partial T^4}{\partial y},$$

where σ* is the Stefan-Boltzman constant and k* is the mean absorption coefficient. Further, we assume that the temperature difference within the flow is such that T^4 is expressed as a linear function of temperature. Hence, expanding T^4 in Taylor series about T_∞ and neglecting higher order terms, we obtain,

$$T^4\cong 4T_\infty^3T-3T_\infty^4.$$

Considering the similarity transformation Yousif et al. (2017).

$$\left.\begin{aligned} &u=a\,x^n f'(\zeta),\ \zeta=y\sqrt{\frac{a(n+1)}{2\nu}}x^{\left(\frac{n-1}{2}\right)},\ v=-\sqrt{\frac{a\nu(n+1)}{2}}x^{\left(\frac{n-1}{2}\right)}\left(f(\zeta)+\frac{n-1}{n+1}\zeta f'(\zeta)\right),\\ &\psi=\sqrt{\frac{2a\nu}{(n+1)}}x^{\left(\frac{n-1}{2}\right)}f(\zeta),\ \theta(\zeta)=\frac{T-T_\infty}{T_w-T_\infty},\ \phi(\zeta)=\frac{C-C_\infty}{C_w-C_\infty}, \end{aligned}\right\} \tag{6}$$

where ζ is the similarity variable, ψ is the stream function, f(ζ) is the dimensionless stream function, θ(ζ) is a dimensionless temperature of the fluid in the boundary layer region, ϕ(ζ) is a dimensionless concentration of the fluid in the boundary layer region.

The stream function ψ is formalized in the standard way as,

$$u=\frac{\partial\psi}{\partial y},\qquad v=-\frac{\partial\psi}{\partial x}$$

Substituting Equation (6) in Equations (2) to (5), we obtain,

$$\left(1+\frac{1}{\beta}\right)f'''+f\,f''-\frac{2}{n+1}f'^2-(M+K_1)f'=0 \tag{7}$$

$$\left(1+\frac{4}{3}R\right)\theta''+\Pr f\theta'+\Pr Nb\theta'\phi'+\Pr Nt\theta'^2+\left(1+\frac{1}{\beta}\right)\Pr Ec f''^2+\Pr Q\theta=0 \tag{8}$$

$$\phi''+\frac{1}{2}Le f\phi'+\frac{Nt}{Nb}\theta''-Le\gamma\phi=0 \tag{9}$$

The boundary conditions are,

$$\begin{aligned} &f=S, \quad f'=1, \quad \theta=1, \quad \phi=1 \quad at \quad \zeta=0,\\ &f'=0, \quad \theta=0 \quad \phi=0 \quad as \quad \zeta\to\infty, \end{aligned} \tag{10}$$

Non-dimensional skin friction coefficient C_f, local Nusselt number Nu_x and local Sherwood number Sh_x are,

$$C_f=\frac{\tau_w}{\rho U_w^2}, \text{ where } \tau_w=\mu_B\left(1+\frac{1}{\beta}\right)\left(\frac{\partial u}{\partial y}\right)_{y=0}, \; Nu_x=\frac{xq_w}{k(T_w-T_\infty)} \text{ and} \tag{11}$$

$$Sh_x=\frac{xq_m}{D_B(C_w-C_\infty)}$$

where k is the thermal conductivity of the nanofluid, q_w and q_m are the heat and mass fluxes at the surface respectively given by,

$$q_w=\left(-\left(k+\frac{16\sigma^* T_\infty^3}{3k^*}\right)\left(\frac{\partial T}{\partial y}\right)\right)_{y=0} \qquad q_m=-D_m\left(\frac{\partial C}{\partial y}\right)_{y=0} \tag{12}$$

Substituting q_w and q_m in the preceding equations, we get

$$\mathrm{Re}_x^{1/2}C_f\sqrt{\frac{2}{n+1}}=\left(1+\frac{1}{\beta}\right)f''(0), \; \mathrm{Re}_x^{-1/2}Nu_x\sqrt{\frac{2}{n+1}}=-\left(1+\frac{4}{3}R\right)\theta'(0) \text{ and}$$

$$\mathrm{Re}_x^{-1/2}Sh_x\sqrt{\frac{2}{n+1}}=-\phi'(0)$$

where $\mathrm{Re}_x=\frac{U_w x}{\nu}$ is the local Reynolds number.

2. HAM Solution

For this intent, we take the initial guesses f_0, θ_0 and ϕ_0 of f, θ and ϕ in the following form

$$\begin{aligned} f_0(\xi)&=S+1-e^{-\xi},\\ \theta_0(\xi)&=e^{-\xi},\\ \phi_0(\xi)&=e^{-\xi}. \end{aligned} \tag{13}$$

The linear operators are selected as

$$\begin{aligned} L_1(f)&=f'''-f',\\ L_2(\theta)&=\theta''-\theta,\\ L_3(\phi)&=\phi''-\phi, \end{aligned} \tag{14}$$

with the following properties

$$\begin{aligned} L_1\left(C_1+C_2e^{\zeta}+C_3e^{-\zeta}\right)&=0,\\ L_2\left(C_4e^{\zeta}+C_5e^{-\zeta}\right)&=0,\\ L_3\left(C_6e^{\zeta}+C_7e^{-\zeta}\right)&=0, \end{aligned}$$

where C_i (i = 1 to 7) are the arbitrary constants.

We construct the zeroth-order deformation equations,

$$(1-p)L_1\left(f(\zeta;p)-f_0(\zeta)\right)=p\hbar_1 N_1\left[f(\zeta;p)\right], \tag{15}$$

$$(1-p)L_2\left(\theta(\zeta;p)-\theta_0(\zeta)\right)=p\hbar_2 N_2\left[f(\zeta;p),\theta(\zeta;p),\phi(\zeta;p)\right], \tag{16}$$

$$(1-p)L_3\left(\phi(\zeta;p)-\phi_0(\zeta)\right)=p\hbar_3 N_3\left[f(\zeta;p),\theta(\zeta;p),\phi(\zeta;p)\right], \tag{17}$$

subject to the boundary conditions,

$$\begin{aligned} &f(0;p)=S, \quad f'(0;p)=1, \quad f'(\infty;p)=1,\\ &\theta(0;p)=1, \qquad\qquad \theta(\infty;p)=0,\\ &\phi(0;p)=1, \qquad\qquad \phi(\infty;p)=0, \end{aligned} \tag{18}$$

where,

$$N_1\left[f(\zeta;p)\right]=\left(1+\frac{1}{\beta}\right)\frac{\partial^3 f(\zeta;p)}{\partial\zeta^3}+f(\zeta;p)\frac{\partial^2 f(\zeta;p)}{\partial\zeta^2}-\frac{2n}{1+n}\left(\frac{\partial f(\zeta;p)}{\partial\zeta}\right)^2-(M+K)\frac{\partial f(\zeta;p)}{\partial\zeta}, \tag{19}$$

$$\begin{aligned} N_2\left[f(\zeta;p),\theta(\zeta;p),\phi(\zeta;p)\right]=&\left(1+\frac{4}{3}R\right)\frac{\partial^2\theta(\zeta;p)}{\partial\zeta^2}+\Pr\left(f(\zeta;p)\frac{\partial\theta(\zeta;p)}{\partial\zeta}\right)+\Pr Nb\,\frac{\partial\theta(\zeta;p)}{\partial\zeta}\frac{\partial\phi(\zeta;p)}{\partial\zeta}+\Pr Nt\left(\frac{\partial\theta(\zeta;p)}{\partial\zeta}\right)^2\\ &+\Pr\left(1+\frac{1}{\beta}\right)Ec\left(\left(\frac{\partial^2 f(\zeta;p)}{\partial\zeta^2}\right)^2\right)+\Pr Q\theta(\zeta;p) \end{aligned} \tag{20}$$

$$N_3\left[f(\zeta;p),\theta(\zeta;p),\phi(\zeta;p)\right]=\frac{\partial^2\phi(\zeta;p)}{\partial\zeta^2}+\frac{1}{2}Le\,f(\zeta;p)\frac{\partial\phi(\zeta;p)}{\partial\zeta}+\frac{Nt}{Nb}\frac{\partial^2\theta(\zeta;p)}{\partial\zeta^2}-Le\gamma\phi(\zeta;p). \tag{21}$$

where $p\in[0,1]$ is the embedding parameter, h_1, h_2 and h_3 are non-zero auxiliary parameters and N_1, N_2 and N_3 are nonlinear operators.

The m^{th}-order deformation equations are follows

$$L_1\left(f_m(\zeta)-\chi_m f_{m-1}(\zeta)\right)=\hbar_1 R_m^f(\zeta), \tag{22}$$

$$L_2\left(\theta_m(\zeta)-\chi_m\theta_{m-1}(\zeta)\right)=\hbar_2 R_m^\theta(\zeta), \tag{23}$$

$$L_3\left(\phi_m(\zeta)-\chi_m\phi_{m-1}(\zeta)\right)=\hbar_3 R_m^\phi(\zeta), \tag{24}$$

with the following boundary conditions

$$\begin{aligned} &f_m(0)=0, \quad f_m'(0)=0, \quad f_m'(\infty)=0,\\ &\theta_m(0)=0, \qquad\qquad \theta_m(\infty)=0,\\ &\phi_m(0)=0, \qquad\qquad \phi_m(\infty)=0, \end{aligned} \tag{25}$$

where,

$$R_m^f(\zeta)=\left(1+\frac{1}{\beta}\right)f_{m-1}'''+\left[\sum_{i=0}^{m-1}f_{m-1-i}f_i'''-\frac{2n}{n+1}\left(\sum_{i=0}^{m-1}f_{m-1-i}'f_i'\right)-(M+K)f_{m-1}'\right], \tag{26}$$

$$R_m^\theta(\xi)=\left(1+\frac{4}{3}R\right)\theta_{m-1}''+Pr\sum_{i=0}^{m-1}f_{m-1-i}\theta_i'+\Pr Nb\sum_{i=0}^{m-1}\theta_{m-1-i}'\phi_i'+\Pr Nt\sum_{i=0}^{m-1}\theta_{m-1-i}'\theta_i'+\Pr\left(1+\frac{1}{\beta}\right)Ec\sum_{i=0}^{m-1}f_{m-1-i}''f_i'''+\Pr Q\theta_{m-1}, \tag{27}$$

$$R_m^\phi(\xi)=\phi_{m-1}''+\frac{1}{2}Le\sum_{i=0}^{m-1}f_{m-1-i}\phi_i'+\frac{Nt}{Nb}\theta_{m-1}''-\gamma\,Le\,\phi_{m-1} \tag{28}$$

$$\chi_m=\begin{cases}0, & m\le 1,\\ 1, & m>1.\end{cases} \tag{29}$$

3. Convergence of HAM solution

The higher deformation equations corresponding to Equations (7) to (9) subject to the boundary conditions (10) can be

formulated using above initial guesses and linear operators and the appropriate values for the non-zero parameters h_1, h_2 and h_3 have been obtained by plotting the h-curves in Figure 1. From the Figure, it is seen that the valid regions of h_1, h_2 and h_3 are about [-1.1, -0.1]. For $h_1=h_2=h_3=-0.62$ our results are in good correlation with the existing results. Table 1 displays the convergence of adopted method.

4. Results and Discussion

In this article, we studied the heat and mass transfer characteristics of Casson nanofluid over a nonlinear stretching sheet. The arising mathematical problem is governed by interesting parameters which include Casson fluid parameter (β), nonlinear parameter (n), magnetic parameter (M), porous parameter (K_1), suction parameter (S), thermal radiation (R), Prandtl number (Pr), Brownian motion parameter (Nb), thermophoresis parameter (Nt), viscous dissipation (Ec), heat source parameter (Q), Lewis number (Le) and chemical reaction parameter (γ). Numerical solutions are carried out through HAM. The obtained results are displayed through graphs and tabular forms. In the present study following default parameter values are adopted for computations:

$$\beta=1.0, n=\Pr=Le=2.0,\ M=Nb=0.5, R=S=K_1=Q=0.1, Nt=0.3, Ec=\gamma=0.2.$$

All graphs therefore correspond to these values unless specifically indicated in the appropriate graph.

The effect of magnetic parameters on velocity, temperature, and concentration are depicted in Figures 2, 3, and 4. Velocity drops as the magnetic parameter M increases, but temperature and concentration have the reverse effect. The Lorentz force created by the magnetic field is responsible for this. Figures 5, 6 and 7 illustrate the influence of Casson fluid parameter β on velocity, temperature and concentration profiles. Increase of Casson fluid parameter β, increases the viscosity of the fluid and as a result velocity decreases. It is also observed that temperature increases and concentration decelerates with the increase of β.

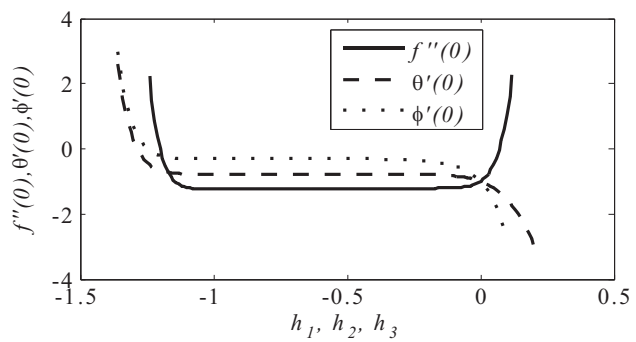

Figure 1. h-curves of f''(0), θ'(0) and ϕ'(0) for 15th Order Approximation

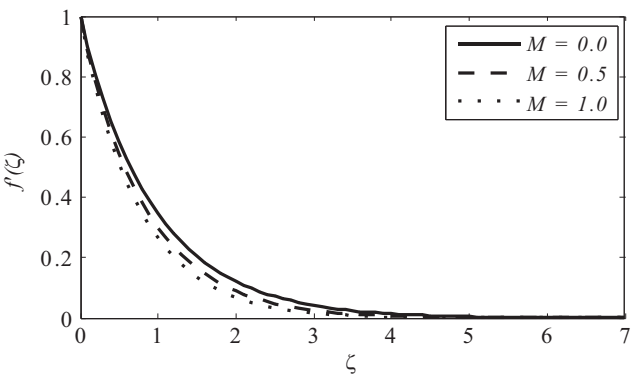

Figure 2. Impact of M on f'(ξ)

Order	-f''(0)	-θ'(0)	-ϕ'(0)
5	1.955455	0.210933	0.993088
10	1.955552	0.222725	0.995894
15	1.955553	0.222615	0.994708
20	1.955553	0.222597	0.994487
25	1.955553	0.222593	0.994437
30	1.955553	0.22592	0.94425
35	1.955553	0.222592	0.994421
40	1.955553	0.22592	0.994421
45	1.955553	0.222592	0.994421

Table 1. Convergence of HAM Solution for Different Orders of Approximations when $\beta=1.0, n=\Pr=Le=2.0,\ M=Nb=0.5, R=S=K_1=Q=0.1, Nt=0.3, Ec=\gamma=0.2.$

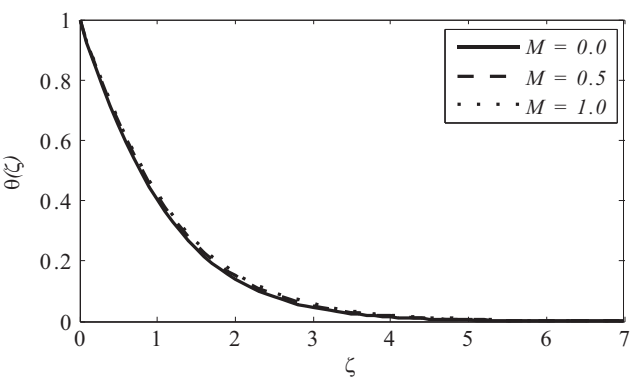

Figure 3. Impact of M on θ(ξ)

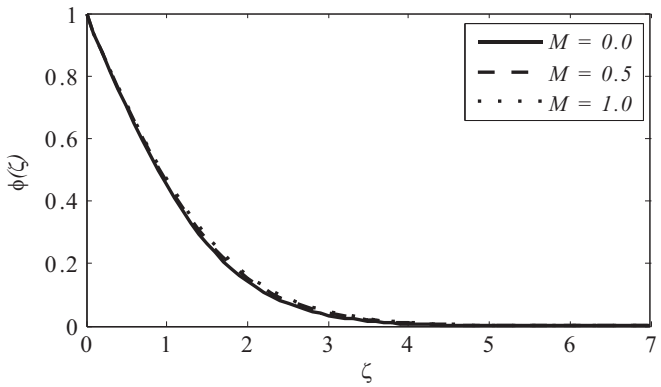

Figure 4. Impact of M on ϕ(ξ)

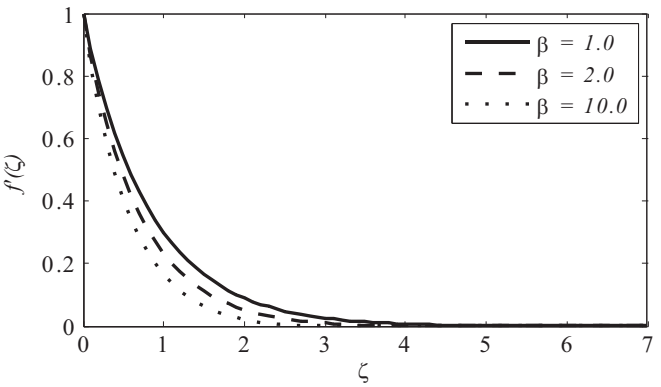

Figure 5. Impact of β on f'(ξ)

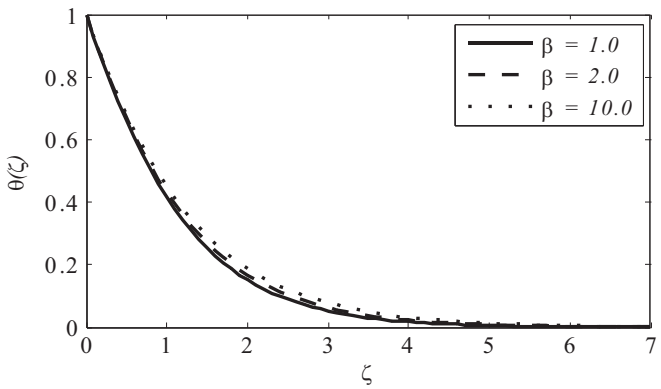

Figure 6. Impact of β on θ(ξ)

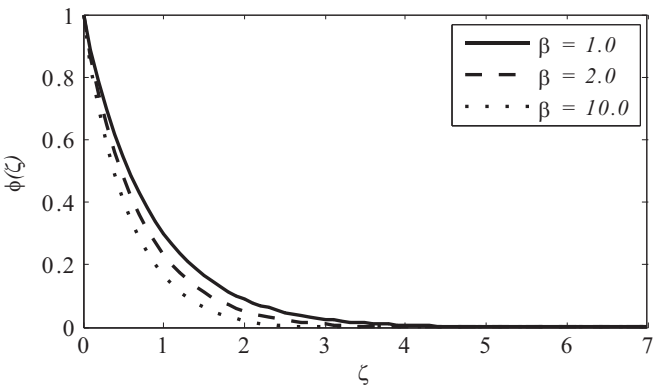

Figure 7. Impact of β on ϕ(ξ)

Figures 8, 9 and 10 illustrate velocity, temperature, and concentration patterns for various nonlinear stretching parameter values. With the growth of the nonlinear parameter n, velocity falls while temperature and concentration increase. Suction S causes the fluid to move closer to the surface, reducing momentum, thermal boundary layer thickness, and concentration boundary layer thickness. Figures 11, 12, and 13 depict this.

An increase in the fluid's viscosity, a drop in the permeability at the edge, or a fall in the stretching rate of the accelerating surface causes a rise in the porosity parameter, resulting in a gradual decrease in the fluid's flow velocity. The temperature profile shows the opposite behaviour for different values of the porosity parameter. Figures 14 to 16 depict this.

Figure 17 depicts the effect of the radiation parameter R on temperature. It has been observed that as R increases, the temperature rises. The reason for this is because as the amount of heat energy released into the fluid increases, the

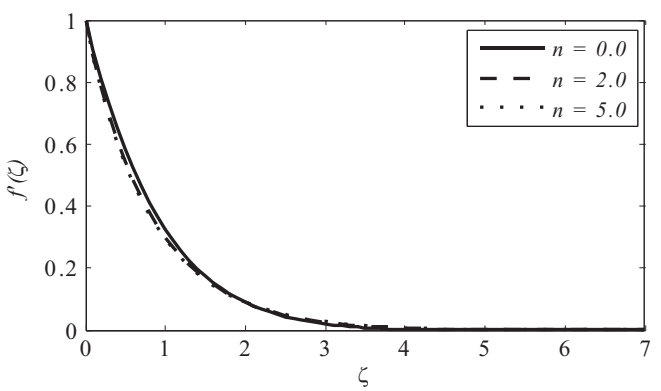

Figure 8. Outcome of n on f'(ξ)

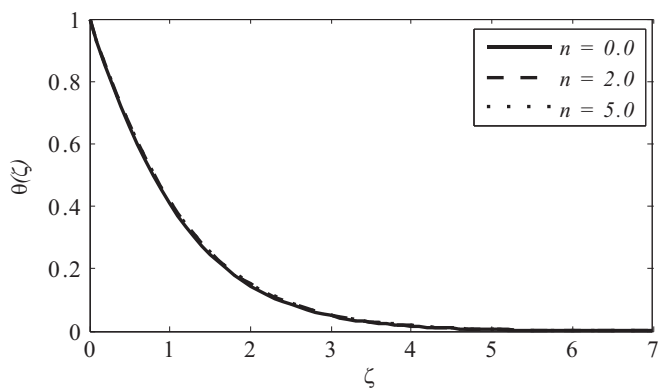

Figure 9. Impact of n on θ(ξ)

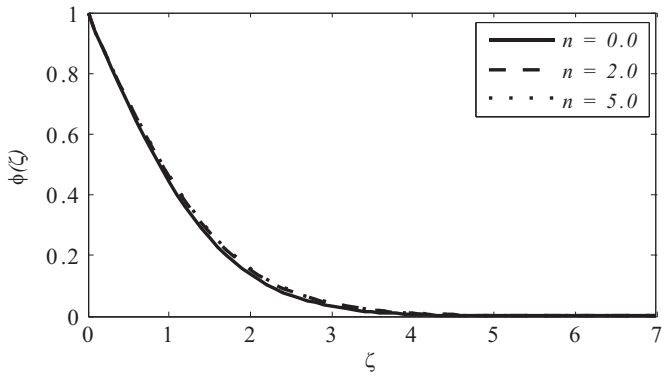

Figure 10. Effect of n on $\phi(\xi)$

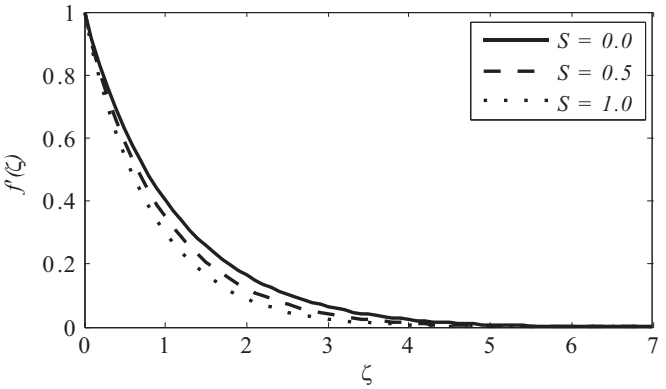

Figure 11. Impact of S on f'(ζ)

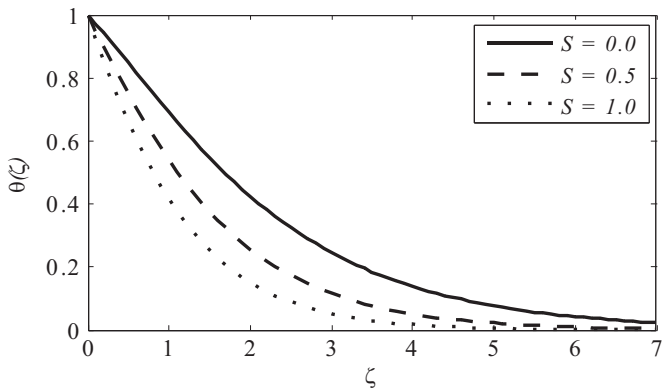

Figure 12. Impact of S on $\theta(\zeta)$

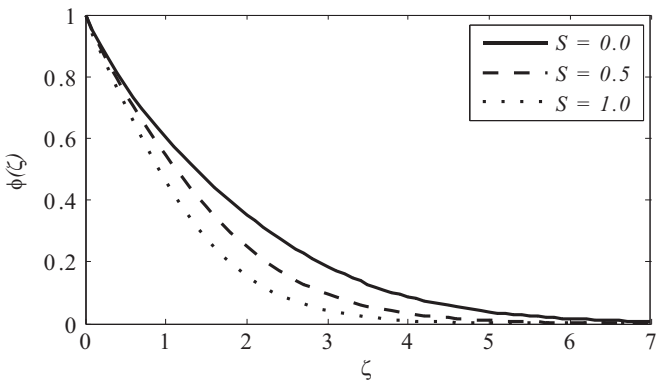

Figure 13. Effect of S on $\phi(\zeta)$

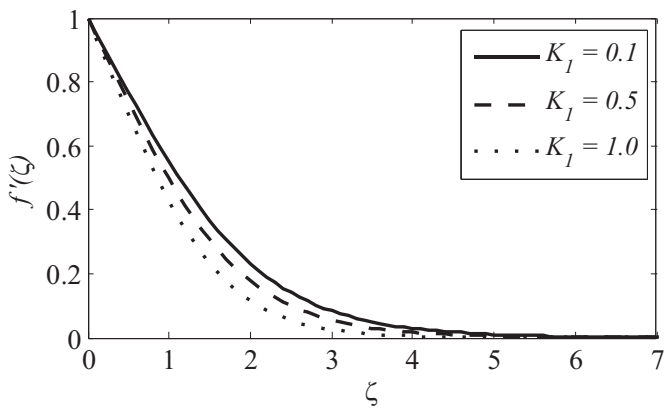

Figure 14. Effect of K_1 on f'(ζ)

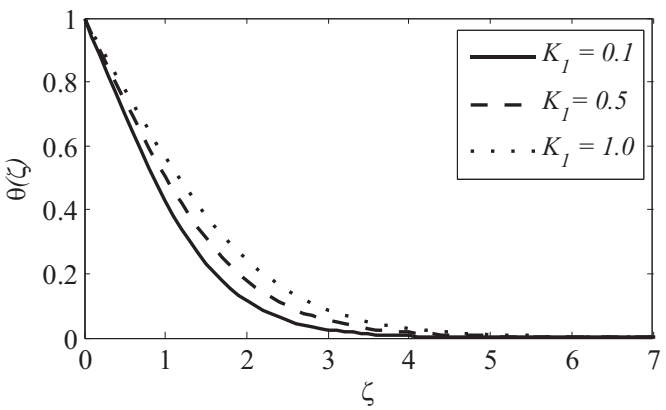

Figure 15. Effect of K_1 on $\theta(\zeta)$

temperature rises. When greater Prandtl number Pr values are used, heat dispersion away from the heated surface is much slower than when smaller Prandtl values are used. As a result, as illustrated in Figure 18, temperature drops as the Prandtl number rises.

Figure 19 depicts the effect of the Eckert number Ec on temperature. The temperature of the wall rises as the amount of heat added by frictional heating rises. The effect of the heat source/sink parameter Q on temperature is seen in Figure 20. The temperature drops for negative values of (heat sink) due to heat absorption in the thermal boundary layer, as seen in the graph. Similarly, with positive values of (heat source), heat generation happens in the thermal boundary layer, and therefore temperature rises.

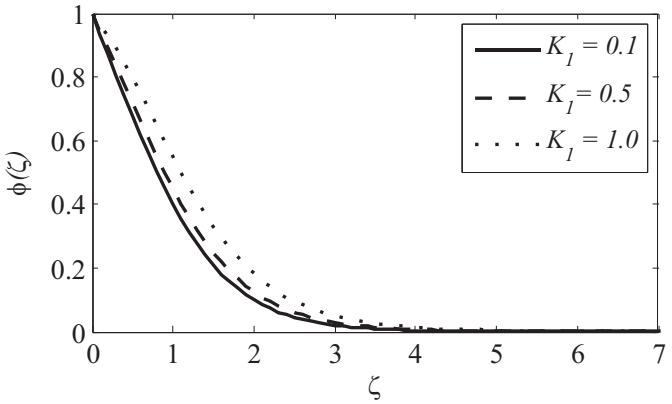

Figure 16. Effect of K_1 on $\phi(\zeta)$

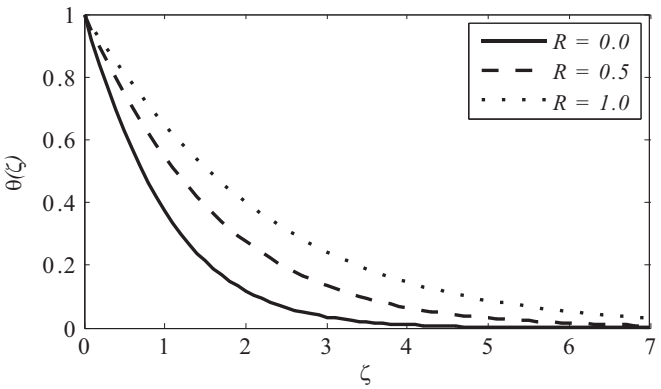

Figure 17. Effect of R on $\theta(\xi)$

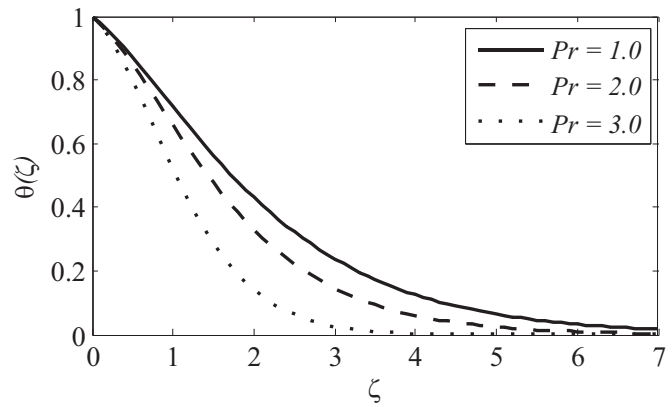

Figure 18. Effect of Pr on $\theta(\zeta)$

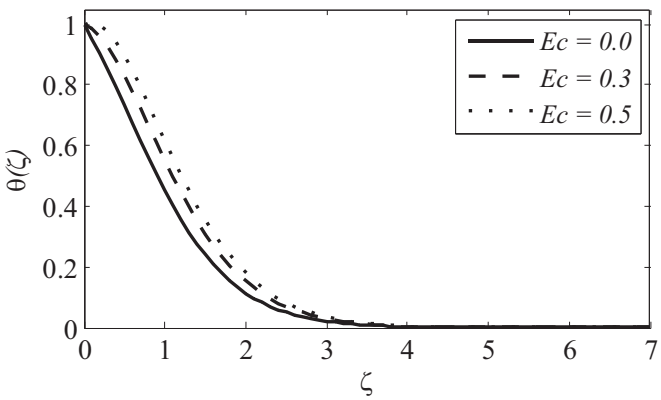

Figure 19. Impact of Ec on $\theta(\xi)$

Figures 21 and 22 reveal the implications of the Brownian motion parameter Nb on temperature and concentration fields. Brownian motion, in general, helps to heat the fluid in the boundary layer and limit particle deposition away from the fluid on the surface. As a direct consequence, the temperature goes up while the concentration lowers. The inclusion of nanoparticles externally allowed the thermophoresis parameters Nt to appear. Thermal conductivity of liquid is associated with the presence of nanoparticles. While we use higher intensity of Nt, the thermal conductivity of liquid boosts and this elevated thermal conductivity lead to a higher temperature. We also identified that relatively high Nt values result in greater nanoparticle concentrations. This is shown in Figures 23 and 24.

Figure 25 shows that an increase in Lewis number Le leads to decay in nanoparticles concentration distribution. Schmidt

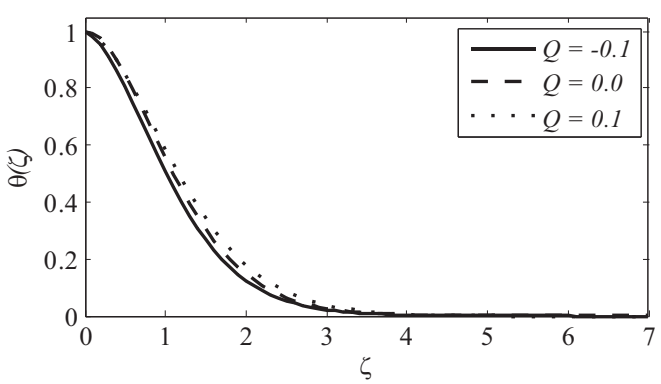

Figure 20. Impact of Q on $\theta(\zeta)$

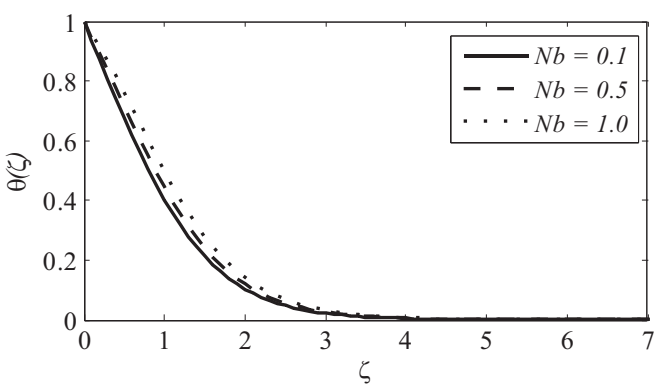

Figure 21. Result of Nb on $\theta(\zeta)$

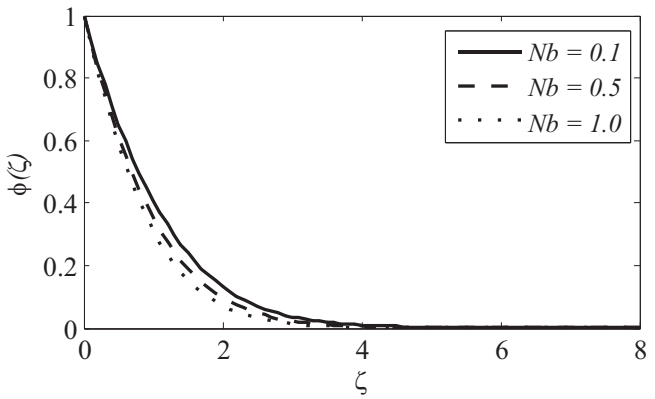

Figure 22. Effect of Nb on $\phi(\zeta)$

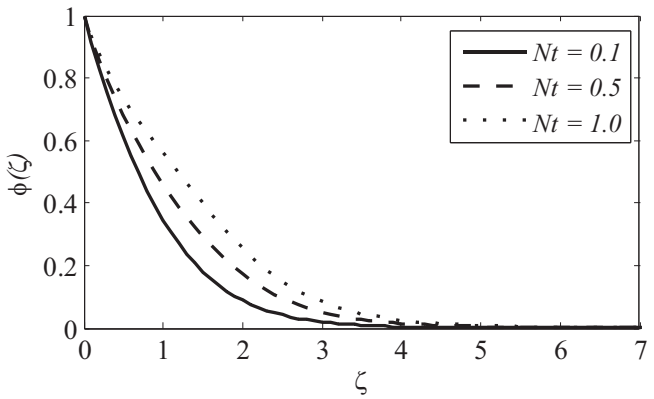

Figure 23. Result of Nt on $\theta(\zeta)$

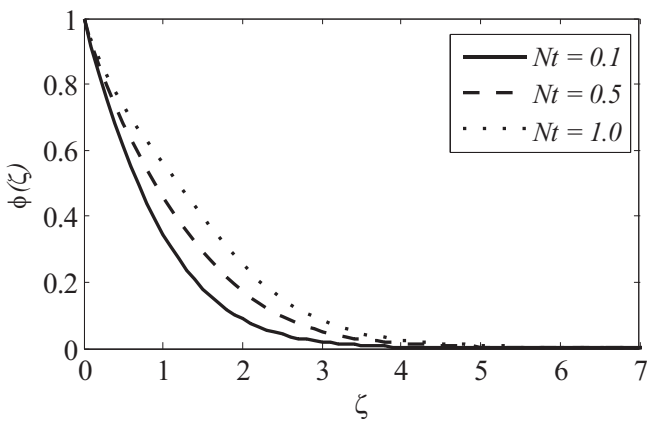

Figure 24. Effect of Nt on $\theta(\zeta)$

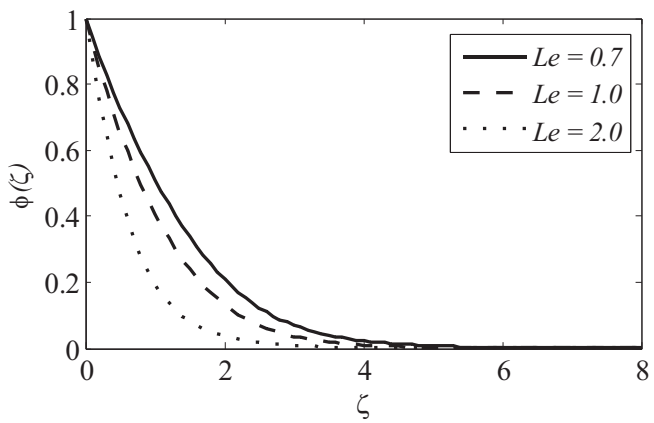

Figure 25. Effect of Le on $\phi(\xi)$

number has an inverse relationship with the Brownian diffusion coefficient. Larger values of Lewis number Le correspond to a weaker Brownian diffusion coefficient, which causes reduction in nanoparticles concentration distribution. Stronger chemical reaction parameter leads to lower nanoparticle concentration, as shown in Figure 26. This phenomenon is explained by the fact that destructive chemical rate increases mass transfer rate, resulting in a drop in nanoparticle concentration.

Local Nusselt number amplifies with R but reduces with β. This is noticed in Figure 27. Assessments of $-\theta'(0)$ and $\phi'(0)$ with recently existing literature are undertaken in Table 2, and the stats indicate a strong and positive correlation.

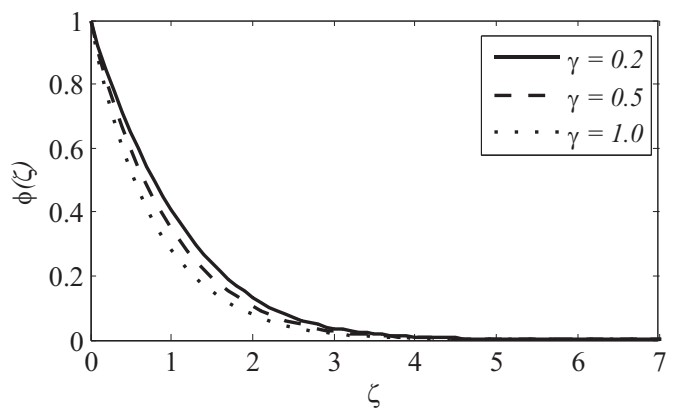

Figure 26. Effect of γ on $\phi(\xi)$

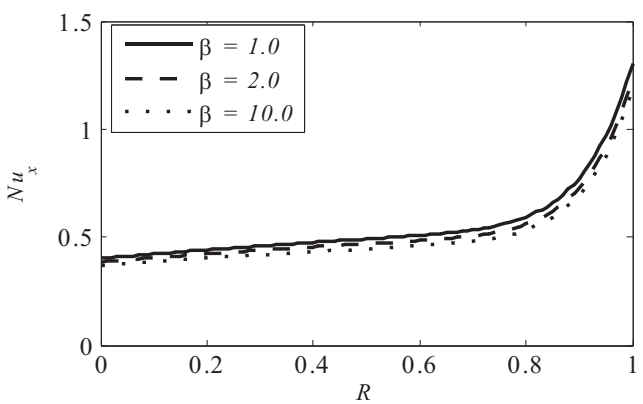

Figure 27. Effect of β and R on Nu_x

n	Nt	$-\theta'(0)$	$-\phi'(0)$	$-\theta'(0)$	$-\phi'(0)$	$-\theta'(0)$	$-\phi'(0)$
0.2	0.3	0.4533	0.8395	0.4520	0.8402	0.452019	0.840133
	0.5	0.3999	0.8048	0.3987	0.8059	0.399937	0.805741
3.0	0.3	0.4282	0.7785	0.4271	0.7791	0.427223	0.779103
	0.5	0.3786	0.8323	0.3775	0.7390	0.377607	0.738916

Table 2. Comparison of Local Nusselt Number and Local Sherwood Number when $M=K_1=S=R=Ec=Q=\gamma=0.0$, $Nb=0.5$, $Pr=Le=2.0$ and $\beta\to\infty$

Conclusions

In this paper, a boundary layer analysis of MHD flow of Casson nanofluid over a nonlinear porous stretching sheet is presented. The use of Casson nanofluid makes this analysis a unique one. From this study the following conclusions are made:

- Momentum boundary layer becomes thinner as increase β, M, n.
- Temperature acts as an increasing function of R, Ec, Nb, Nt.
- Nanoparticle volume fraction enhances with Nt.
- Local Nusselt number decreases with β

References

[1]. Abel, M. S., Sanjayanand, E., & Nandeppanavar, M. M. (2008). Viscoelastic MHD flow and heat transfer over a stretching sheet with viscous and ohmic dissipations. *Communications in Nonlinear Science and Numerical Simulation*, 13(9), 1808-1821. https://doi.org/10.1016/j.cnsns.2007.04.007

[2]. Ajayi, T. M., Omowaye, A. J., & Animasaun, I. L. (2017). Viscous dissipation effects on the motion of Casson fluid over an upper horizontal thermally stratified melting surface of a paraboloid of revolution: boundary layer analysis. *Journal of Applied Mathematics*. https://doi.org/10.1155/2017/1697135

[3]. Asghar, S., Mohyuddin, M. R., & Hayat, T. (2005). Effects of Hall current and heat transfer on flow due to a pull of eccentric rotating disks. *International Journal of Heat and Mass Transfer*, 48(3-4), 599-607. https://doi.org/10.1016/j.ijheatmasstransfer.2004.08.023

[4]. Choi, S. U., & Eastman, J. A. (1995). *Enhancing Thermal Conductivity of Fluids with Nanoparticles*. Argonne National Lab, United States.

[5]. Dash, R. K., Mehta, K. N., & Jayaraman, G. (1996). Effect of yield stress on the flow of a Casson fluid in a homogeneous porous medium bounded by a circular tube. *Applied Scientific Research*, 57, 133-149.https://doi.org/10.1007/BF02529440

[6]. F. Mabood, W. A., Khan., & A. I. Ismail, (2015). MHD stagnation point flow and heat transfer impinging on stretching sheet with chemical reaction and transpiration. *Chemical Engineering Journal*, 273, 430-437. https://doi.org/10.1016/j.cej.2015.03.037

[7]. Hayat, T., Shehzad, S. A., & Alsaedi, A. (2012). Soret and Dufour effects on magnetohydrodynamic (MHD) flow of Casson fluid. *Applied Mathematics and Mechanics*, 33, 1301-1312. https://doi.org/10.1007/s10483-012-1623-6

[8]. Ibrahim, S. M., Kumar, P. V., & Lorenzini, G. (2020). Analytical modeling of heat and mass transfer of radiative MHD Casson fluid over an exponentially permeable stretching sheet with chemical reaction. *Journal of Engineering Thermophysics*, 29, 136-155. https://doi.org/10.1134/S181023282001010

[9]. Ibrahim, S. M., Kumar, P. V., & Makinde, O. D. (2018, November). Chemical reaction and radiation effects on non-Newtonian fluid flow over a stretching sheet with non-uniform thickness and heat source. In *Defect and Diffusion Forum* (Vol. 387, pp. 319-331). Trans Tech Publications Ltd. https://doi.org/10.4028/www.scientific.net/DDF.387.319

[10]. Ibrahim, S. M., Kumar, P. V., Lorenzini, G., & Lorenzini, E. (2019). Influence of Joule heating and heat source on radiative MHD flow over a stretching porous sheet with power-law heat flux. *Journal of Engineering Thermophysics*, 28, 332-344. https://doi.org/10.1134/S1810232819030044

[11]. Ibrahim, S. M., Lorenzini, G., Kumar, P. V., & Raju, C. S. K. (2017). Influence of chemical reaction and heat source on dissipative MHD mixed convection flow of a Casson nanofluid over a nonlinear permeable stretching sheet. *International Journal of Heat and Mass Transfer*, 111, 346-355. https://doi.org/10.1016/j.ijheatmasstransfer.2017.03.097

[12]. Khan, A. A., Zaimi, K., & Ying, T. Y. (2020). Stagnation point flow of Williamson nanofluid towards a permeable stretching/shrinking sheet with a partial slip. *CFD Letters*, 12(6), 39-56.

[13]. Kumar, G. C., Reddy, K. J., Konijeti, R. K., & Reddy, M. N. (2018, November). Non-uniform heat source/sink and joule heating effects on chemically radiative MHD mixed convective flow of micropolar fluid over a stretching sheet in porous medium. In *Defect and Diffusion Forum* (Vol. 388, pp. 281-302). Trans Tech Publications Ltd. https://doi.org/10.4028/www.scientific.net/DDF.388.281

[14]. Kumar, P. V., Ibrahim, S. M., & Jyothsna, K. (2019). Numerical modeling on radiative dissipative MHD flow of a chemically casson fluid over an exponentially inclined stretching surface. *Mathematical Modelling of Engineering Problems*, 6(4). https://doi.org/10.18280/mmep.060403

[15]. Kumar, P. V., Ibrahim, S. M., & Lorenzini, G. (2017). Impact of thermal radiation and Joule heating on MHD mixed convection flow of a Jeffrey fluid over a stretching sheet using homotopy analysis method. *International Journal of Heat and Technology*, 35(4), 978-986. https://doi.org/10.18280/ijht.350434

[16]. Kumar, P. V., Ibrahim, S. M., & Lorenzini, G. (2018). The study of three dimensional radiative mhd casson nanofluid over an exponential porous stretching sheet with heat source under convective boundary conditions. *International Journal of Heat and Technology*, 36(1), 1-10. https://doi.org/10.18280/ijht.360101

[17]. Kumar, P. V., Ibrahim, S. M., & Lorenzini, G. (2021). Investigation of the heat transfer and flow characteristics on Hiemenz flow under the influence of heat source and thermal radiation with hydrodynamic-thermal slips effects. *Journal of Mechanical Engineering Research and Developments*, 44(9), 369-383.

[18]. Kumaran, V., Banerjee, A. K., Kumar, A. V., & Vajravelu, K. (2009). MHD flow past a stretching permeable sheet. *Applied Mathematics and Computation*, 210(1), 26-32. https://doi.org/10.1016/j.amc.2008.10.025

[19]. Liao, S. (2012). *Homotopy Analysis Method in Nonlinear Differential Equations*. Beijing: Higher Education Press, (pp. 153-165).

[20]. Mabood, F., Ibrahim, S. M., Kumar, P. V., & Khan, W. A. (2017a). Viscous dissipation effects on unsteady mixed convective stagnation point flow using Tiwari-Das nanofluid model. *Results in Physics*, 7, 280-287. https://doi.org/10.1016/j.rinp.2016.12.037

[21]. Mabood, F., Ibrahim, S. M., Lorenzini, G., & Lorenzini, E. (2017b). Radiation effects on Williamson nanofluid flow over a heated surface with magneto hydrodynamics. *International Journal of Heat and Technology*, 35(1), 196-204. https://doi.org/10.18280/ijht.350126

[22]. Mabood, F., Khan, W. A., & Ismail, A. M. (2015). MHD boundary layer flow and heat transfer of nanofluids over a nonlinear stretching sheet: a numerical study. *Journal of Magnetism and Magnetic Materials*, 374, 569-576. https://doi.org/10.1016/j.jmmm.2014.09.013

[23]. Mabood, F., Khan, W. A., & Ismail, A. M. (2017). MHD flow over exponential radiating stretching sheet using homotopy analysis method. *Journal of King Saud University-Engineering Sciences*, 29(1), 68-74. https://doi.org/10.1016/j.jksues.2014.06.001

[24]. Masuda, H., Ebata, A., Teramae, K., & Hishinuma, N. (1993). Alteration of thermal conductivity and viscosity of liquid by dispersing ultra-fine particles (dispersion of-Al_2O_3, SiO_2 and TiO_2 ultra-fine particles). *Netsu Bussei,* 7(4), 227-233.

[25]. Mohyuddin, M. R., & Götz, T. (2005). Resonance behaviour of viscoelastic fluid in Poiseuille flow in the presence of a transversal magnetic field. *International Journal for Numerical Methods in Fluids*, 49(8), 837-847. https://doi.org/10.1002/fld.1026

[26]. Mohyuddin, M. R., & Rizwan, S. M. (2015). Similarity having perturbation in Newtonian fluid. *i-manager's Journal on Mathematics*, 4(4), 22-27. https://doi.org/10.26634/jmat.4.4.3697

[27]. Mopuri, O., Ganteda, C., Mahanta, B., & Lorenzini, G. (2022a). MHD heat and mass transfer steady flow of a convective fluid through a porous plate in the presence of multiple parameters. *Journal of Advanced Research in Fluid Mechanics and Thermal Sciences*, 89(2), 56-75. https://doi.org/10.37934/arfmts.89.2.5675

[28]. Mopuri, O., Kodi, R., Ganteda, C., Srikakulapu, R., & Lorenzini, G. (2022b). MHD heat and mass transfer steady flow of a convective fluid through a porous plate in the presence of diffusion thermo and aligned magnetic field. *Journal of Advanced Research in Fluid Mechanics and Thermal Sciences*, 89(1), 62-76. https://doi.org/10.37934/arfmts.89.1.6276

[29]. Mukhopadhyay, S. (2013). Casson fluid flow and heat transfer over a nonlinearly stretching surface. *Chinese Physics B*, 22(7), 074701. https://doi.org/10.1088/1674-1056/22/7/074701

[30]. Mustafa, M., & Khan, J. A. (2015). Model for flow of Casson nanofluid past a non- linearly stretching sheet considering magnetic field effects. *American Institute of Physics Advances*, 5(7). https://doi.org/10.1063/1.4927449

[31]. N. Casson, A flow equation for pigment oil suspensions of the printing ink type. In: Mill CC, *Rheology of Disperse Systems*, 84-104.

[32]. Nadeem, S., Haq, R. U., & Akbar, N. S. (2013). MHD three-dimensional boundary layer flow of Casson nanofluid past a linearly stretching sheet with convective boundary condition. *IEEE Transactions on Nanotechnology*, 13(1), 109-115. https://doi.org/10.1109/TNANO.2013.2293735

[33]. Pop, E. (2010). Energy dissipation and transport in nanoscale devices. *Nano Research*, 3, 147-169. https://doi.org/10.1007/s12274-010-1019-z

[34]. Rana, P., & Bhargava, R. (2012). Flow and heat transfer of a nanofluid over a nonlinearly stretching sheet: a numerical study. *Communications in Nonlinear Science and Numerical Simulation*, 17(1), 212-226. https://doi.org/10.1016/j.cnsns.2011.05.009

[35]. Rao A. S., Rao, P. P. B., & Ganteda, C. K. (2020). Magnetohydrodynamic Williamson fluid motion over an exponentially stretching sheet with chemically radiative heat source effects under suction/injection. *Journal of Mathematics and Computer Science*, 10(6), 2634-2657.

[36]. Reddy, C. A., & Shankar, B. (2016). MHD stagnation point flow in a boundary layer of a nano fluid over a stretching sheet in the presence of viscous dissipation and chemical reaction. Mechanics, *Materials Science & Engineering Journal*, 1-45.

[37]. Reddy, P. S., & Sreedevi, P. (2021). MHD boundary layer heat and mass transfer flow of nanofluid through porous media over inclined plate with chemical reaction. *Multidiscipline Modeling in Materials and Structures*, 17(2), 317-336. https://doi.org/10.1108/MMMS-03-2020-0044

[38]. Yousif, M. A., Hatami, M., Mahmood, B. A., & Rashidi, M. M. (2017). Thermal boundary layer analysis of nanofluid flow past over a stretching flat plate in different transpiration conditions by using DTM-Padé method. *Journal of Mathematics and Computer Science*, 17(1), 84-95. https://doi.org/10.22436/jmcs.017.01.08

ABOUT THE AUTHORS

Seetharam Karanamu, Department of Mathematics, Aditya Institute of Technology and Management, Tekkali, Srikakulam, Andhra Pradesh, India.

Jayaramireddy Konda is Chief Executive Officer at Science City, Government of Andhra Pradesh, Tadepalli, Guntur District, Andhra Pradesh, India.

Shaik Kalesha Vali, Department of Basic Science & Humanities and Social Sciences, JNTUK University College of Engineering Vizianagaram, Dwarapudi, Vizianagaram, Andhra Pradesh, India.